THE ASTROPHYSICAL JOURNAL, 330:809–816, 1988 July 15

THE DISTANCE TO THE CENTER OF THE GALAXY: H_2O MASER PROPER MOTIONS IN SAGITTARIUS B2(N)

M. J. REID, M. H. SCHNEPS, J. M. MORAN, AND C. R. GWINN
Harvard-Smithsonian Center for Astrophysics

R. GENZEL
Max-Planck-Institut für Physik und Astrophysik

D. DOWNES
Institut de Radio Astronomie Millimetrique

AND

B. RÖNNÄNG
Onsala Space Observatory

Received 1987 October 26; accepted 1988 January 13

ABSTRACT

We measured the proper motions of many H_2O maser spots associated with the star-forming region, Sgr B2(N), which lies close to the Galactic Center. We used five VLBI observations spanning 1.5 yr and achieved relative positional accuracies of about 20 microarcseconds (μas) across a 4″ field, yielding relative transverse velocities with uncertainties of a few km s^{-1}.

The proper motion information shows that the dominant motions of the Sgr B2(N) masers are expansion, with evidence for some rotation. We have modeled the source as an expanding (and rotating) flow and estimated parameters including the source distance, the expansion center, and the expansion and rotation velocities by fitting the kinematic data in a least-squares sense. The expansion velocity is $\sim$45 km s^{-1}, suggesting that the outflow in Sgr B2(N) is more energetic than the outflow associated with IRc2 in Orion. The rotation velocity at a radial distance of 1″ is $\sim$20 km s^{-1}, indicating a mass enclosed by the 2″ masing region of $\sim 2 \times 10^4 M_{\odot}$.

We find the distance to the Sgr B2(N) H_2O masers, and hence the distance to the Galactic Center (R_0), to be 7.1 kpc with a one standard deviation uncertainty, including systematic sources of error, of 1.5 kpc.

Subject headings: galaxies: The Galaxy — galaxies: nuclei — interferometry — interstellar: molecules — masers — stars: proper motions

I. INTRODUCTION

The distance to a star-forming region can be determined by measuring the proper motions within a cluster of H_2O maser spots surrounding a newly formed star. Velocity components toward the observer are determined from Doppler shifts, and angular motions across the plane of the sky are measured by very long baseline interferometric (VLBI) imaging. Since, in the context of a geometric model, the transverse velocities are related to the line-of-sight velocities, the distance to the maser cluster can be determined by comparison of the angular and line-of-sight velocities. Results for the H_2O masers associated with Orion-IRc2 (Genzel *et al.* 1981*a*) and with W51 (Genzel *et al.* 1981*b*; Schneps *et al.* 1981) have demonstrated the power of this technique. Distance measurements in principle can be used to estimate R_0, the distance from the Sun to the center of the Galaxy. For example, the W51 distance of 7 kpc, determined from H_2O proper motions, yields $R_0 = 10.8 \pm 4.8$ kpc (see the Appendix for details).

Three strong sources of H_2O maser emission are seen toward the giant molecular cloud Sgr B2. Since Sgr B2 is close to the dynamical center of the Galaxy, a measurement of the distance to any of the H_2O maser clusters yields *a direct estimate of* R_0. Because of the fundamental importance of R_0 in astrophysics, we conducted a series of VLBI observations of Sgr B2 and other galactic H_2O maser sources designed to measure their internal proper motions. In this paper we present our results for the northernmost H_2O source in Sgr B2, denoted Sgr B2(N).

II. OBSERVATIONS AND DATA ANALYSIS

We conducted VLBI observations on 1980 December 10, 1981 March 31 and December 1, and 1982 March 8 and June 7. Four telescopes in the United States were used: the Haystack 37 m telescope in Westford, Massachusetts; the NRAO 43 m telescope in Green Bank, West Virginia; one of the VLA 25 m telescopes near Socorro, New Mexico; and the OVRO 40 m telescope in Big Pine, California. Receivers at telescopes usually employed maser preamplifiers, and typical total system temperatures were 150 K for the low elevations of the Sgr B2(N) observations.

Figure 1 is a total power spectrum of the Sgr B2(N) H_2O maser taken during the first observations with the Haystack telescope. For the VLBI observations we recorded three 2 MHz bands, centered at local standard of rest velocities, v_{LSR}, of 31, 56, and 81 km s^{-1} (assuming a rest frequency of 22235.080 MHz for the H_2O transition) on the MkII video cassette system by switching every second among the three bands (i.e., time multiplexing with a 3 s cycling period). We chose not to record a fourth frequency band known on occasion to contain weak features with LSR velocities near 113 km s^{-1}. The recorded data were processed on the NRAO MkII correlator in Charlottesville, Virginia, mostly between

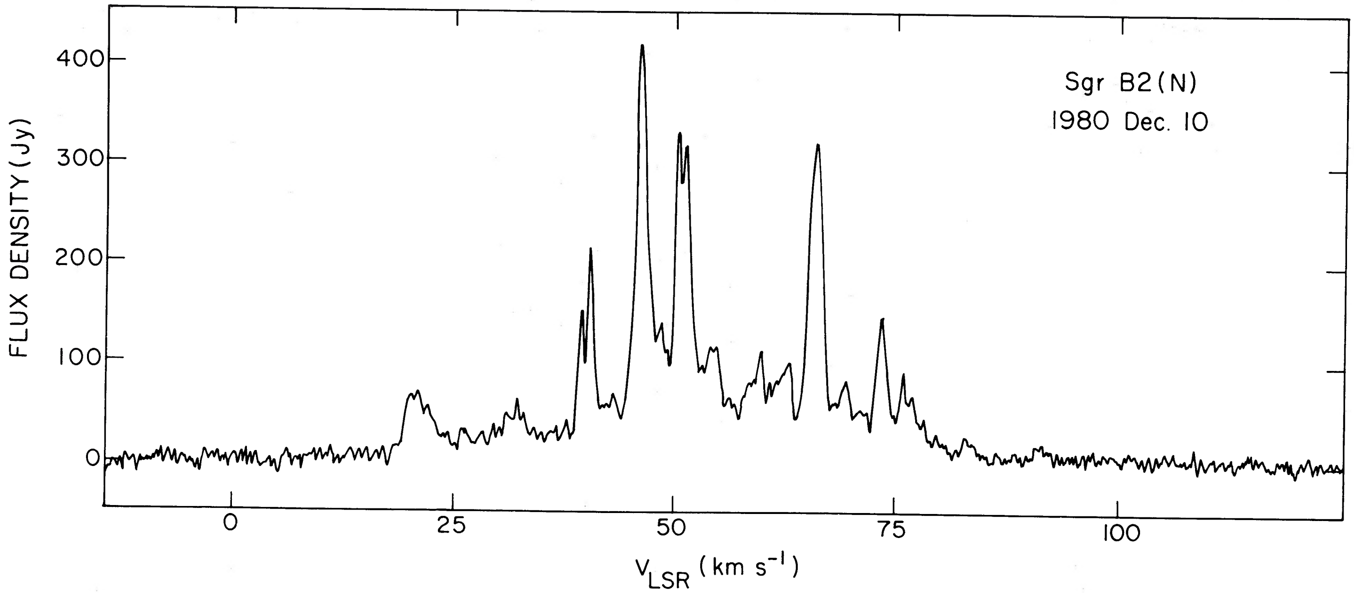

FIG. 1.—Total power spectrum of the H_2O maser emission from Sgr B2(N) as a function of LSR velocity (based on a rest frequency of 22235.080 MHz). The spectrum was taken with the Haystack telescope during the first epoch observations. The flux density scale may be uncertain by 30%. The $\sim 90''$ telescope beam includes the Sgr B2(M) maser source; hence some components are not from Sgr B2(N). At different epochs maser emission from Sgr B2(N) spans a velocity range from ~ 15 to ~ 115 km s^{-1}.

1981 and 1983. The correlator yielded 96 point spectra of cross-correlations and autocorrelations, affording 25 kHz resolution for uniform weighting of the correlation functions.

The 1 s averaged data for each band were calibrated in both amplitude and phase using procedures described by Reid *et al.* (1980). Observations of compact continuum sources (e.g., QSOs) with positions known to better than $\sim 0\farcs01$ were used to determine the locations of the telescopes (to better than 1 m), the absolute position of the maser source (to $\sim 0\farcs1$), and the offsets of the hydrogen-maser clocks for each station (to ~ 10 ns). Corrections for atmospheric propagation effects assumed an elevation-dependent zenith delay (for each site) with a seasonal component for the "wet" term. Values of polar motion and UT1-UTC from the Bureau International de l'Heure (BIH) Circular D were adopted.

Systematic errors in the determination of the positions of individual maser spots *relative to a single reference maser spot* caused by errors in the interferometer-source geometry, station clocks, and atmospheric model are less than 10 microarcseconds (μas). The absolute position of the reference feature at 41.0 km s^{-1} was found to be: R.A.(1950) = $17^h44^m10\fs283 \pm 0\fs003$, Decl.(1950) = $-28°21'16\farcs97 \pm 0\farcs06$. The same reference maser spot was employed for maps at all five epochs. Many systematic sources of error remain constant over the series of observations and, hence, cancel when motions are determined by differencing positions at different epochs. The largest nonconstant source of systematic error probably comes from variations in the atmosphere and station clocks at approximately the 10 nsec level. These variations are not accounted for in the simple models we use and result in nonrepeatable systematic errors in the determination of relative positions of about 10 μas for maser spots separated by 2 MHz (~ 27 km s^{-1}) in Doppler shift.

Crude maps of the locations of all maser spots for each epoch were made by fringe-rate mapping techniques (see Walker *et al.* 1981; Thompson, Moran, and Swenson 1986). Maser spots stronger than about 3 Jy were detectable in this manner, and positions accurate to better than 5 milliarcseconds (mas) were obtained. Synthesis maps were made at all five epochs at the position of any spot detected (even if the spot was detected at only one epoch) for the spectral channel in which the spot was detected and also for the adjacent spectral channels. The calibrated interferometer data were phase-shifted to the position determined by fringe-rate mapping and then analyzed using the Astronomical Image Processing System (AIPS) software from NRAO. Maps covering ± 19 mas in the right ascension and declination directions were made and "cleaned." The synthesized interferometer beam had a full-width at half-maximum of 0.4 mas east–west by 2.4 mas north–south. A two-dimensional Gaussian model for the intensity distribution was fitted to significant peaks in these maps. The central position of the Gaussian model defined the maser spot position at the epoch of observation. All positions were then converted to epoch 1950 coordinates, to account for differential precession, nutation, and aberration, and corrected for gravitational deflection by the Sun prior to determining motions. We estimate that uncertainties in the relative positions from the effects across the 4" field are ~ 1 μas.

III. RESULTS

Maps for individual spectral channels typically had an rms noise level of 0.1 Jy giving a secure detection threshold of slightly less than 1 Jy. Most maps exhibited a dynamic range of about 10 to 1 (peak intensity to rms sidelobe) which limited our ability to find weak spots close to (i.e., within ~ 20 mas of) stronger spots. However, it is unlikely that we failed to identify many *independent* masers motions, since (1) the dynamic range limit applies only to maser spots with nearly the same LSR velocity as well as sky position and (2) when two maser spots were located close to each other they typically exhibited similar three-dimensional motions and were considered part of the same physical condensation when proper motions were analyzed.

Figure 2 displays plots of position versus time for a sample

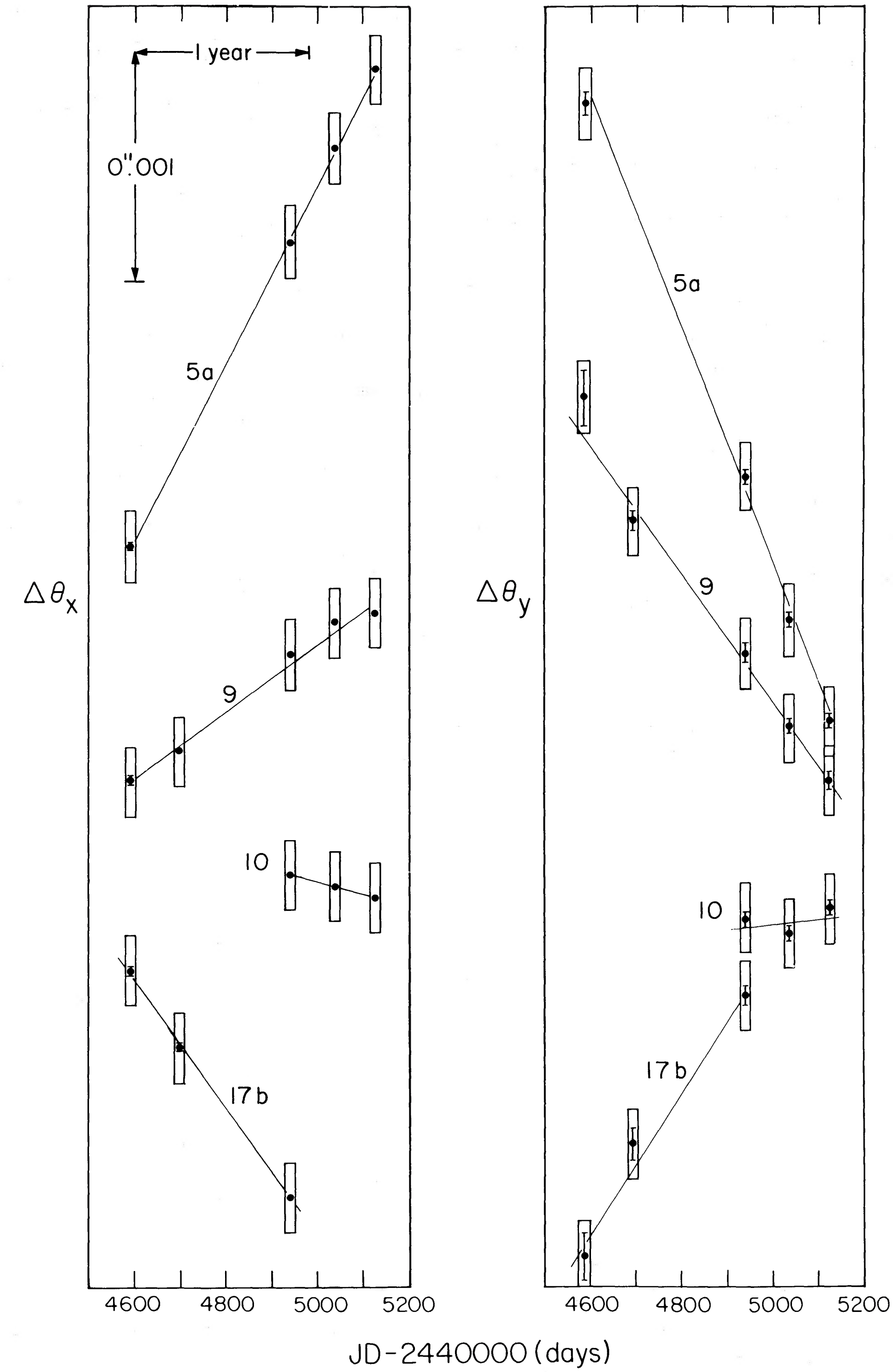

FIG. 2.—Examples of proper motions of H_2O maser spots in Sgr B2(N). Plotted are eastward (*left-hand panel*) and northward (*right-hand panel*) positions measured with respect to a reference maser feature as a function of time. A vertical scale of 1 mas is indicated in the upper left-hand corner. The data points are plotted with error bars and enclosed in rectangular boxes. In some cases the error bars are smaller than the symbol indicating the position of the maser spot. The vertical size of the rectangular boxes is 0.3 mas, a characteristic size of the maser spots. The horizontal size of the boxes is arbitrary.

of maser spots. The spatial-temporal "matrix" of maser spots was sufficiently sparsely populated that incorrect pairing of maser spots at different epochs is highly unlikely. Only maser spots (1) with the same LSR velocity and (2) whose positions at different epochs implied motions of less than 200 km s^{-1} in *both* the right ascension and declination directions (for an *a priori* source distance of 8 kpc) were considered as proper motion candidates.

We determined motions for all spectral channels by fitting straight lines to the right ascensions and declinations as a function of time. In the fitting procedure all data were variance weighted according to their expected position uncertainty, σ_θ, given by the formula

$$\sigma_\theta = \left(\frac{4}{\pi}\right)^{1/4} \frac{\theta}{\sqrt{8 \ln 2}} \frac{\sigma_S}{S}, \tag{1}$$

where θ is the apparent full-width at half-maximum size, and S and σ_S are the peak and rms flux density, respectively, of the maser spot in the map. Usually similar proper motions were derived for many nearly contiguous spectral channels. Since the proper motions from such channels probably reflect the motion of a single physical maser condensation, we averaged them together and report only the averaged motion here. The spectrum of a single physical condensation sometimes was more complex than a single spectral line, probably due in part to the presence of hyperfine splitting of the H_2O line (cf. Walker 1984). We assigned the intensity-weighted average of the line profile as the LSR velocity of the condensation. Table 1 gives the locations and motions of the 24 maser condensations for which we were able to determine motions.

The maser motions are well modeled as moving along straight line trajectories. The deviations of the measured maser positions from a best-fit straight line to the position versus time data are small, typically ~20 μas. Deviations of this magnitude cause velocity errors of a few km s^{-1}. These deviations are within a factor of 2 of those expected from signal-to-noise considerations and nonreproducible systematic errors (e.g., clock errors). Also, it is possible that refractive effects in the interstellar medium cause a wandering of the apparent differential position of maser spots (Gwinn *et al.* 1988).

The H_2O proper motions in Sgr B2(N) are illustrated in Figure 3. The maser spots predominantly trace an expanding flow, presumably from a newly formed star (or stars) near the position indicated by the X in the map. Such spot motions are analogous to the H_2O maser outflow asociated with Orion IRc2 (Genzel *et al.* 1981*a*). The angular extent of detectable H_2O maser spots in Sgr B2(N) is about 4″, compared to about 60″ for Orion IRc2, consistent with Sgr B2(N) being roughly 15 times more distant than the Orion Nebula.

The Sgr B2(N) H_2O proper motion vectors in Figure 3 also indicate departures from a uniform spherical outflow which greatly exceed the measurement errors of typically a few km s^{-1}. This result suggests a "turbulent" velocity component of

TABLE 1

SAGITTARIUS B2(N) H_2O MASER DATA

Id[a]	No. of chans[b]	$\Delta\theta_x$[c]	$\Delta\theta_y$[d]	v_x[e]	σ_{v_x}[f]	v_y[g]	σ_{v_y}[h]	v_z[i]	σ_{v_z}[j]
1	7	0.000	0.000	−1.2	0.1	−1.4	0.3	41.0	0.1
2	17	0.057	−0.004	−6.3	0.2	5.7	1.3	65.2	0.2
3[k]	2	−2.172	−0.237	16.	5.	−52.	30.	74.6	5.
4	1	−2.053	−0.100	10.0	0.6	−40.5	3.6	47.8	0.6
5a	17	−2.053	−0.280	54.1	0.2	−72.6	1.3	36.3	0.2
5b	2	−2.034	−0.272	52.7	2.6	−22.7	15.3	31.7	2.6
6	18	−2.046	−0.303	20.0	0.1	−55.2	0.4	22.5	0.1
7	1	−1.974	−0.105	22.1	2.5	−54.1	15.0	56.0	2.5
9	14	−1.931	−0.113	16.3	0.2	−39.4	1.5	69.8	0.2
10	6	−2.619	0.144	−9.3	0.4	8.3	2.3	92.1	0.4
15	2	−2.914	1.458	−79.1	2.3	72.5	99.9	50.4	2.3
17a	2	−2.836	1.596	−85.1	1.3	25.3	7.7	77.5	1.3
17b	1	−2.831	1.594	−36.9	2.3	38.8	13.7	76.5	2.3
18	3	−1.133	2.199	−31.9	0.3	29.6	2.0	57.1	0.3
19[k]	2	−2.087	0.004	31.	5.	−58.	30.	44.0	5.
21	3	−2.091	−0.128	10.4	4.2	−25.0	24.9	38.3	4.2
24	2	−2.007	−0.084	21.2	3.1	−10.9	18.9	50.0	3.1
25	1	−2.115	−0.152	31.8	3.7	−38.5	22.0	57.7	3.7
26	2	−2.262	−0.219	−9.8	5.5	−54.4	33.2	88.5	5.5
27[k]	3	−2.428	0.792	−20.	5.	−24.	30.	59.1	5.
29[k]	3	−2.129	0.681	−28.	5.	−7.	30.	22.6	5.
31	2	−2.428	0.793	−11.6	1.4	−14.9	8.6	59.3	1.4
35	2	−2.960	0.001	−41.0	2.9	−17.6	17.6	71.6	2.9
36[k]	2	−4.019	1.029	−41.	5.	−53.	30.	78.5	5.

[a] Maser feature identifier.
[b] Number of spectral channels averaged together.
[c] x-offset in arcsec eastward from reference feature position of R.A.(1950) = 17^{h}44^{m}10^s.283.
[d] y-offset in arcsec northward from reference feature position of Decl.(1950) = −28°21′16″.97.
[e] x-velocity for *a priori* distance of 8 kpc (km s^{-1}).
[f] Measurement uncertainty in v_x (km s^{-1}).
[g] y-velocity for *a priori* distance of 8 kpc (km s^{-1}).
[h] Measurement uncertainty in v_y (km s^{-1}).
[i] z-velocity (i.e., v_{LSR}) (km s^{-1}).
[j] Estimated uncertainty in v_z (km s^{-1}).
[k] Maser feature detected only at two epochs.

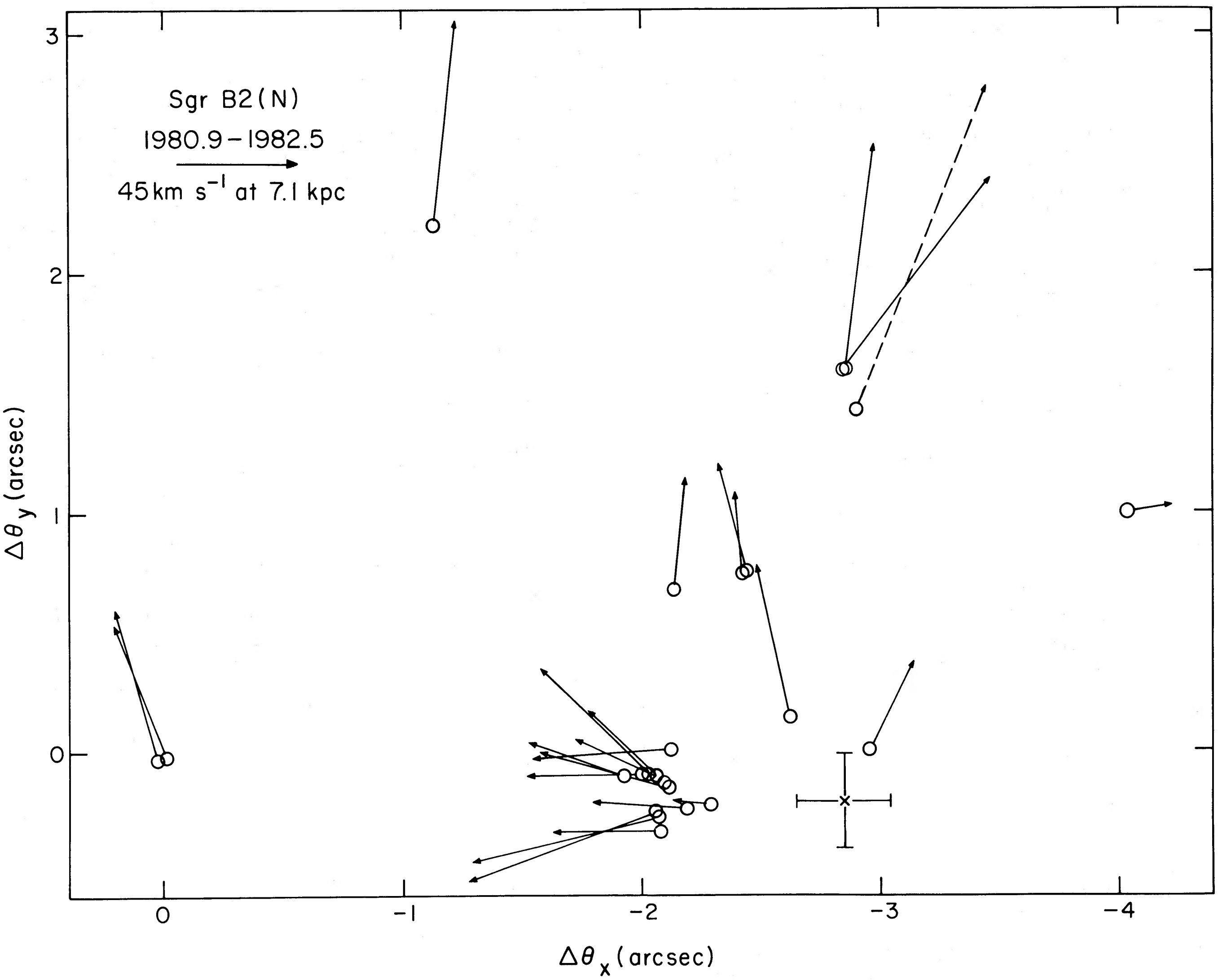

FIG. 3.—Proper motions of the H_2O masers in Sgr B2(N). Circles indicate the positions of maser spots on the sky with north upward and east leftward; the size of the circles is much greater than the maser spot size and is arbitrary. The length and orientation of the arrows indicate the speeds and directions of the maser features, respectively. The length of the horizontal arrow in the upper left-hand corner of the figure corresponds to a speed of 45 km s^{-1} for a source distance of 7.1 kpc. The motions plotted are from Table 1 with the velocity offsets (v_{x_0}, v_{y_0}) listed in Table 2 subtracted. The center of expansion and its uncertainty is indicated by the X symbol and surrounding error bars.

about 15 km s^{-1} (in each dimension), which is similar to, but smaller than, that of the H_2O masers in the source W51(M) (Genzel *et al.* 1981*b*). Many maser spots varied greatly in strength between observations 3 months apart. Thus, although ~ 50 maser spots could be detected at one epoch, less than half that number could be detected on the two or more epochs needed to measure motions. The characteristic time for the maser spots to vary by more than a factor of 2 is comparable to the sound crossing time of the amplification length of $\sim 10^{14}$ cm (see Tarter and Welch 1986). This result suggests that conditions for strong maser amplification may be linked to the conditions which give rise to the significant turbulence observed in the motions.

IV. THE KINEMATIC MODEL

The distance to an expanding H_2O maser source can be estimated from proper motion and radial velocity data (Genzel *et al.* 1981*a*). We take as observable data the three components of velocity (v_x, v_y, and v_z), and as independent variables the sky positions (x and y). For a uniform outflow we must solve for seven global parameters: the source distance, D; the expansion velocity, $V_{\rm exp}$; the three components of the velocity of the center of expansion with respect to the reference feature, v_{x0}, v_{y0}, and v_{z0}; and the sky position of the center of expansion, x_0, and y_0. In addition the z-coordinate (i.e., radial coordinate) offset, z, of the maser spot from the center of the flow must be estimated. Explicitly, the model for a uniformly expanding flow is

$$v_x = \frac{V_{\rm exp}}{d}\frac{(x - x_0)}{R} + v_{x0}\,, \tag{2}$$

$$v_y = \frac{V_{\rm exp}}{d}\frac{(y - y_0)}{R} + v_{y0}\,, \tag{3}$$

$$v_z = V_{\rm exp}\frac{z}{R} + v_{z0}\,, \tag{4}$$

where $R = [(x - x_0)^2 + (y - y_0)^2 + z^2]^{1/2}$. In this formulation, the source distance is given by $D_0 d$ where D_0 is the *a priori* source distance (assumed when converting angular to linear motions) and d is a dimensionless parameter.

This model can be generalized by adding other terms to equations (2), (3), and (4). For example, a component of velocity due to "solid body" rotation can be included by adding $v_{x_{\rm rot}}$, $v_{y_{\rm rot}}$, and $v_{z_{\rm rot}}$ to the right-hand side of equations (2), (3), and (4), respectively, where

$$v_{x_{\rm rot}} = -V_{\rm rot}(y \cos \alpha \cos \beta - z \sin \beta) , \quad (5)$$

$$v_{y_{\rm rot}} = V_{\rm rot}(x \cos \alpha - z \sin \alpha) \cos \beta , \quad (6)$$

$$v_{z_{\rm rot}} = -V_{\rm rot}(x \sin \beta - y \sin \alpha \cos \beta) . \quad (7)$$

In the above equations, $V_{\rm rot}$ is the rotation speed at a distance of 1″ from the rotation axis which is tilted by an angle α about the y-axis and an angle β about the (rotated) x-axis.

a) Initial Estimates of Parameters

The following procedure was used to provide initial estimates for the parameters assuming uniform expansion of the source (i.e., eqs. [2], [3], and [4]).

1. Adjust v_{x0} and v_{y0} so that the proper motion vectors referenced to the center-of-outflow (i.e., $v_x - v_{x0}$) best converge back to a single sky position (x_0, y_0).
2. Estimate v_{z0} and $V_{\rm exp}$ from the midpoint and width of the radial velocity spectrum, respectively, or from other molecular line data.
3. Solve the v_z equation for the z-parameter for each maser feature.
4. Plot $(x - x_0)/R$ versus $(v_x - v_{x0})/V_{\rm exp}$ and measure the slope which gives the x-component distance parameter estimate. A similar plot for the y-component data yields another distance estimate.

The radial velocity of the center of the outflow, v_{z0}, is well established by recent high-resolution observations of NH_3 at the VLA (Vogel, Genzel, and Palmer 1987) and of SO with the Hat Creek millimeter-wavelength interferometer (J. Carlstrom, private communication). These studies detected strong molecular emission from a compact cloud with the same position and extent as the H_2O masers. Both the NH_3 and SO lines peak at 64 km s^{-1} with respect to the LSR, which is also the midpoint of the H_2O maser spectrum. Because of the similarities in extent, position, and velocity of the NH_3, SO, and H_2O molecules, it is likely they are components of the same physical cloud with an LSR velocity $v_{z0} = 64$ km s^{-1}.

The expansion velocity, $V_{\rm exp}$, can be estimated from the width of the H_2O maser spectrum. The H_2O spectrum of Sgr B2(N) contains features from $v_{\rm LSR}$ of about 15 to 115 km s^{-1}. This is well centered on the adopted v_{z0} of 64 km s^{-1} and indicates an expansion velocity of close to 50 km s^{-1}. We would then expect $V_{\rm exp} = 45$ km s^{-1}, which allows for some broadening of the spectrum from nonradial motions. Following steps 1 through 4 above yields the following initial estimates for the other five global parameters: $D = D_0 d = 7.9$ kpc, $v_{x0} = -25$ km s^{-1}, $v_{y0} = -25$ km s^{-1}, $x_0 = -2''67$, and $y_0 = 0''00$. We note that this is not the optimum solution. The process needs to be iterated and all parameters adjusted simultaneously as described in § IV*b* below.

b) Final Parameter Estimates

We examined the residuals to the initial fit for systematic trends that might indicate a deficiency in the uniformly expanding model. A plot of the proper motion residuals on the map of the source indicated that the maser spots appeared to have a measurable component of rotation. The rotation speed appeared greater for maser spots farther from the center of expansion. Therefore, we generalized the model to include the components of velocity due to "solid-body" rotation given by equations (5), (6), and (7). Solid body rotation is appropriate for a constant-density mass distribution.

The fitting procedure minimizes the sum of the squares of the "observed-minus-model" weighted residuals. Three aspects of the fitting process deserve mention: First, based upon our experience with other H_2O maser sources and also from the residuals to the initial fit, we expect turbulent motions intrinsic to the source [$\sim$15 km s^{-1} for Sgr B2(N); see discussion below] to exceed the measurement uncertainties (typically 3 km s^{-1}). Therefore, we assigned weights to the velocity data by combining the measurement uncertainties in quadrature with 15d km s^{-1} for v_x and v_y and 15 km s^{-1} for v_z data. Thus, the relative weighting of the proper motion and radial velocity data depends on the distance estimate. Second, in order to restrict the parameter estimates to physically reasonable values as well as to incorporate our knowledge of some parameters, we added *a priori* weights to the solutions. This allowed us to incorporate the information that $v_{z0} = 64 \pm 3$ km s^{-1}, based upon other molecular data (see discussion above). Other parameter estimates were assigned large *a priori* uncertainties (e.g., $V_{\rm exp} = 45 \pm 30$ km s^{-1} and $D = 8.5 \pm 3.5$ km s^{-1}) so as not to overly constrain the solutions. Third, the z-offset from the center of expansion (z-parameter) appears directly in the v_z data equation, but only weakly in the proper motion data equations through R (see eqs. [2] through [4]). Thus, there are more degrees of freedom associated with the v_z data equations than with the v_x and v_y equations. In practice this allows the least-squares minimization technique to "overfit" the v_z data by having nearly one adjustable parameter per equation. Therefore, we attempted solutions both in the standard manner and also by incorporating a constraint on the set of z-parameters. The constraint chosen was to make the average magnitude of the z-parameters equal to the average magnitude of the x- and y-offsets from the center of expansion.

The global parameters and the z-parameters for each maser spot were adjusted to minimize the sum of the squares of the weighted residuals. Table 2 gives the best estimates for the global parameters of the expanding-rotating model. The expansion speed is more than twice that seen in the "low-velocity" outflow in the Orion H_2O maser. Assuming similar densities are required to excite the H_2O masers in both sources, this suggests a more energetic outflow for Sgr B2(N). The (solid-body) rotation speed of 20 km s^{-1} at a 1″ radius ($\sim 10^{17}$ cm) indicates that the mass enclosed by the masing region (2″ radius) is $\sim 2 \times 10^4\ M_\odot$. This is close to the mass of $\sim 5 \times 10^3\ M_\odot$ estimated by Vogel, Genzel, and Palmer (1987) for the Sgr B2(N) core based upon NH_3 observations. Assuming at most a small number of O stars excite the H_2O masers, nearly all of the mass enclosed by the masing region is not contained in stars, but is still in the molecular cloud material out of which the exciting star(s) formed.

V. THE DISTANCE TO THE GALACTIC CENTER

In addition to the parameter estimates, we calculated formal errors for the parameters of the expanding-rotating model. While formal errors take into account parameter correlations, they can in some cases underestimate the uncertainties often

TABLE 2

KINEMATIC MODEL OF SAGITTARIUS B2(N) H_2O MASERS

Parameter[a]	Best Value	Uncertainty[b]	Units	Comment
D	7.1	± 1.5	kpc	Distance to source
$\Delta\theta_{x_0}$	-2.85	± 0.2	arcsec	Center of expansion[c]
$\Delta\theta_{y_0}$	-0.20	± 0.2	arcsec	
v_{x_0}	-23	± 10	km s^{-1}	Velocity offsets
v_{y_0}	-55	± 11	km s^{-1}	
v_{z_0}	63	± 3	km s^{-1}	
V_{exp}	45	± 9	km s^{-1}	Expansion speed
V_{rot}	20	± 6	km s^{-1}	Rotation speed at 1″ radius
α	0.2	± 0.2	radians	Orientation of rotation axis
β	-0.6	± 0.2	radians	

[a] See test for definitions.

[b] Estimated 1 σ uncertainty including systematic errors.

[c] Offsets (east and north) from reference position of R.A.(1950) = $17^h44^m10^s.283 \pm 0^s.003$, Decl.(1950) = $-28°21'16''.97 \pm 0''.06$.

associated with fitting real data with a simple mathematical model. In order to assess the sensitivity of the distance estimate to different treatments of the data, we ran a series of solutions in which we did or did not use (1) *a priori* weights, (2) the z-parameter constraint (discussed above), (3) rotation in the model, and (4) certain data points. Estimated one standard-deviation uncertainties for the parameters based upon the formal errors and the parameter variations seen in the different treatments of the data are given in Table 2. In general, the variations of the parameters in the series of solutions were less than the formal errors for the parameters.

The distance parameter (d) exhibited correlation coefficients of up to ~ 0.8 with the expansion (V_{exp}) and rotation (V_{rot}) speed parameters. The correlation of d with V_{exp} occurs because the parameters appear as a ratio in the proper motion equations (2) and (3), and because of the need to solve for the z-parameters in equation (4). The formal error for the distance parameter typically was about 20% of the estimated distance. The range of distance parameter estimates for the different treatments of the data clustered near 7 kpc and varied between 5 and 8 kpc in these tests. We conclude that the best estimate of the distance to Sgr B2(N) and one standard-deviation uncertainty is

$$D = 7.1 \pm 1.5 \text{ kpc} . \tag{8}$$

In principle the "velocity ellipsoid" of the post-fit residuals contains information about the source distance. Provided that random motions of the maser spots are the dominant component in the velocity residuals, the dispersion of the v_x and v_y residuals can be compared to the dispersion of the v_z residuals to obtain a statistical parallax. In practice, however, estimating the z-parameters "over-fits" the v_z data and reduces the dispersion of its residuals compared to the v_x and v_y data. We tested this effect on simulated data and found the rms of the v_z residuals typically was about 60% of the rms of the v_x and v_y residuals. The real data for Sgr B2(N) also exhibited a similar reduction of the radial velocity residuals compared to the proper motion residuals. We feel this gives additional support for the accuracy of our modeling and of the distance estimate.

Several arguments can be given that Sgr B2 is within a few hundred parsecs of the center of the Galaxy. First, Sgr B2 is projected less than 80 pc from the Galactic Center. It would be highly unlikely for such a unique molecular cloud to be at some random distance and by chance projected so close to the Galactic Center. Second, the high LSR velocity of ~ 64 km s^{-1} for Sgr B2(N) can only occur if the cloud is at a galactocentric distance, $R_{\mathrm{Sgr\,B2(N)}}$, given by

$$R_{\mathrm{Sgr\,B2(N)}} < R_0 \frac{\Theta \sin l}{v_{\mathrm{LSR}}} , \tag{9}$$

where we assume circular rotation and where Θ is the rotation speed of the Galaxy and l is the galactic longitude for Sgr B2(N). For $\Theta < 250$ km s^{-1} and $l = 0°.7$, $R_{\mathrm{Sgr\,B2(N)}} < 0.05 R_0$. Third, atomic and molecular absorption studies place Sgr B2 within the "270-pc expanding shell" (Scoville 1972). We conclude that the Sgr B2 cloud containing Sgr B2(N) is within ~ 0.3 kpc of the dynamical center of the Galaxy and that hence our estimate of the distance to Sgr B2(N) implies

$$R_0 = 7.1 \pm 1.5 \text{ kpc} . \tag{10}$$

VI. CONCLUSIONS

We have measured the distance to Sgr B2(N) by modeling the proper motions of the H_2O maser spots. Since Sgr B2 is very close to the Galactic Center, we find $R_0 = 7.1 \pm 1.5$ kpc. This result is two standard deviations lower than the "round number" value of 10 kpc commonly used and one standard deviation lower than the value of 8.5 kpc recently adopted by the IAU (Kerr and Lynden-Bell 1986). The IAU value was obtained by averaging, in an unweighted fashion, previous estimates of R_0. Most of the previous estimates of R_0 rely on knowledge of intrinsic source luminosities and/or extinction to the sources. Our method of measuring distances does not depend on such knowledge and, hence, gives a truly *independent* estimate of the size of the Galaxy.

The following is a list of some of the effects of reducing R_0:

1. decrease all kinematic distances;
2. reduce the mass of the Galaxy and of the Galactic Center;
3. decrease some extragalactic distances (i.e., increase H_0) by:

a. favoring recent revisions of the absolute magnitudes of RR Lyrae variables (Frenk and White 1982) which in turn affect distances in the Local Cluster;

b. bringing spiral galaxies closer to match the Milky Way size (e.g., de Vaucouleurs 1983);

4. decrease the luminous mass in the Milky Way and increase the "dark matter" in the Local Group (see Trimble 1986);

5. reduce the total luminosity of X-ray bursts, some of which appear super-Eddington for $R_0 = 10$ kpc (see Ebisuzaki, Hanawa, and Sugimoto 1984).

Improvements in the distance to the Galactic Center can come from proper motion measurements for the two other strong H_2O masers in the Sgr B2 complex and from the strongest maser source in the Galaxy, W49(N). In particular, W49 is fortuitously located near the Solar Circle ($v_{LSR} = 9$ km s^{-1}); and an estimate of R_0 from its distance is not sensitive to details of the kinematic model of the Galaxy. W49 is a very strong source with hundreds of maser features and data currently being analyzed should yield a very accurate distance.

We thank A. Harris for his help during the observations and J. Burch and R. Vernon for their tireless efforts at the VLBI correlator in Charlottesville.

APPENDIX

Previous H_2O proper motion distance estimates are 0.48 ± 0.08 kpc for the Orion-IRc2 H_2O masers (Genzel *et al.* 1981*a*) and 7.0 ± 1.5 kpc for the W51 H_2O masers (Genzel *et al.* 1981*b*; Schneps *et al.* 1981). The Orion result agrees with optical distance estimates which range from 0.4 to 0.5 kpc; however, this source is too close to the Sun to be used to estimate R_0. The W51 result can be used to determine R_0, but it is very sensitive to the assumed kinematic model of the Galaxy. Given a kinematic distance to a source, D_k, and a measured distance, D, the distance to the center of the Galaxy can be estimated as

$$R_0 = \frac{D}{D_k} R_{0a} , \tag{A1}$$

where R_{0a} is the assumed value of R_0 used to derive the kinematic distance. If $\Theta_0 = 220$ km s^{-1} and $R_{0a} = 8.5$ kpc (IAU values), then circular rotation of the Galaxy gives $v_{LSR} < 53$ km s^{-1} for $l_{W51} = 49\overset{\circ}{.}5$. The measured $v_{LSR} = 57$ km s^{-1} for W51 (Genzel *et al.* 1981*b*) exceeds the maximum velocity allowed by circular rotation and suggests a distance close to the tangent point, i.e., $D_k = 5.5$ kpc. Using this value and the measured distance to W51, equation (A1) yields an estimate of $R_0 = 10.8$ kpc. The uncertainty in this estimate comes mostly from the uncertainty in D_k. Assuming that streaming motions and/or peculiar motions can cause v_{LSR} to differ from pure circular motion by 10 km s^{-1}, and that Θ_0 is uncertain by 20 km s^{-1}, the kinematic distance to W51 can range from 3.5 to 7.5 kpc—that is, $D_k = 5.5 \pm 2.0$ kpc. Combining the uncertainty in the measurement of the distance to W51 and the uncertainty in the estimate of D_k, the uncertainty in the estimate of R_0 via equation (A1) is 4.6 kpc. Thus, the proper motion results for W51 yield $R_0 = 10.8 \pm 4.6$ kpc, a value consistent with the more accurate estimate obtained for Sgr B2(N).

REFERENCES

de Vaucouleurs, G. 1983, *Ap. J.*, **268**, 451.
Ebisuzaki, T., Hanawa, T., and Sugimoto, D. 1984, *Pub. Astr. Soc. Japan*, **36**, 551.
Frenk, C. S., and White, S. D. M. 1982, *M.N.R.A.S.*, **198**, 173.
Genzel, R., *et al.* 1981*b*, *Ap. J.*, **247**, 1039.
Genzel, R., Reid, M. J., Moran, J. M., and Downes, D. 1981*a*, *Ap. J.*, **244**, 884.
Gwinn, C. R., Moran, J. M., Reid, M. J., and Schneps, M. H. 1988, *Ap. J.*, **330**, 817.
Kerr, F., and Lynden-Bell, D. 1986, *M.N.R.A.S.*, **221**, 1023.
Reid, M. J., Haschick, A. D., Burke, B. F., Moran, J. M., Johnston, K. J., and Swenson, G. W. 1980, *Ap. J.*, **239**, 89.
Schneps, M. H., Lane, A. P., Downes, D., Moran, J. M., Genzel, R., and Reid, M. J. 1981, *Ap. J.*, **249**, 124.
Scoville, N. Z. 1972, *Ap. J. (Letters)*, **175**, L127.
Tarter, J. C., and Welch, W. J. 1986, *Ap. J.*, **305**, 467.
Thompson, A. R., Moran, J. M., and Swenson, G. W. 1986, *Interferometry and Synthesis in Radio Astronomy* (New York: Wiley), p. 384.
Trimble, V. 1986, *Comments A.*, **11**, 257.
Vogel, S. N., Genzel, R., and Palmer, P. 1987, *Ap. J.*, **316**, 243.
Walker, R. C. 1981, *A.J.*, **86**, 1323.
———. 1984, *Ap. J.*, **280**, 618.

D. Downes: Institut de Radio Astronomie Millimetrique, Voie 10, Domaine Universitaire, 38406 St. Martin d'Heres, France

R. Genzel: Max-Planck-Institut für Physik und Astrophysik, Karl-Schwarzschild-Str. 1, D-8046 Garching bei München, Federal Republic of Germany

C. R. Gwinn, J. M. Moran, M. J. Reid, and M. H. Schneps: Harvard-Smithsonian Center for Astrophysics, 60 Garden St., Cambridge, MA 02138

B. Rönnäng: Onsala Space Observatory, S-439 00 Onsala, Sweden